32nd URSI GASS, Montreal, 19–26 August 2017

Electromagnetic Scattering by Several 2-D Red Blood Cell Models

Polat Goktas*(1), Ilya O. Sukharevsky(2), and Ayhan Altintas(1)
(1) Department of Electrical and Electronics Engineering, Bilkent University, TR-06800, Bilkent, Ankara, Turkey
(2) Technical University of Munich, Arcisstraße 21, 80333 München, Germany

Abstract

The electromagnetic 2-D scattering from a red blood cell model is analyzed by using Muller boundary integral equation (MBIE) method. The accuracy and smoothness of the solution are improved by applying Nystrom-type discretization. We present numerical results on a single RBC in the different major phases of mitosis. The simulations show that the cell shape, as well as the cell orientation, have a large influence on the scattering properties of RBCs.

1 Introduction

The scattering of electromagnetic waves by dielectric particles is a problem of interest in many applications ranging from remote sensing to radar meteorology and biological sciences [1]. Red blood cells (RBCs), also known as erythrocytes, are the major scattering particles in whole blood due to their dominant volumetric concentration and high scattering cross-section [2]. Scattering cross section values of an RBC provide essential information on the morphological properties of the cell. The boundary IE (BIE) techniques are one of the most popular computational tools in the scattering of waves by 2D homogeneous dielectric bodies, being more economic than volume IE. The spurious eigenvalues are absent for the Muller boundary integral equation (MBIE), which is a pair of coupled second-kind IEs for the field components tangential to the scatterer contour [3], [4]. In this paper, we present a comparative study of scattering from a single healthy RBC. Scattering cross section values for different RBC shapes and different cell orientations are obtained accurately and efficiently using Muller boundary integral equation (MBIE) technique.

2 Problem Formulation and MBIE Method

Consider a two-dimensional model of a blood cell D_i with permittivity, $\varepsilon_i(\lambda)$, permeability, $\mu_i(\lambda)$, and cross-section contour L. The host medium D_e has $\varepsilon_e(\lambda)$, and $\mu_e(\lambda)$, respectively (Figure 1). The time factor $e^{-j\omega t}$ is assumed and suppressed throughout the paper. In a single-shell model, the biological cell is considered as a homogenous conducting particle enclosed in a conducting shell. A brief view of the structures of the diffferent-shaped shell models in a homogeneous suspending medium is depicted in Figure 2, and the equivalent complex permittivity of the cell is calculated by [5]:

$$\varepsilon_i = \varepsilon_{mem}\frac{\gamma^3 + 2\left(\frac{\varepsilon_{cp}-\varepsilon_{mem}}{\varepsilon_{cp}+2\varepsilon_{mem}}\right)}{\gamma^3 - \left(\frac{\varepsilon_{cp}-\varepsilon_{mem}}{\varepsilon_{cp}+2\varepsilon_{mem}}\right)} \quad (1)$$

with $\gamma = 1 + d/R$, where ε_{mem} and ε_{cp} are the complex permittivities of the cell membrane and cytoplasm, respectively. R is the radius of the cell and d is the membrane thickness. The boundary contour of a blood cell at different stages of cell division can be properly parametrized in polar coordinates by Cassini's oval [6]:

$$r(\theta) = \sqrt{b^2\cos 2\theta + \sqrt{b^4\cos^2 2\theta + a^4 - b^4}}. \quad (2)$$

By varying parameters a, b in (2), we obtain boundaries from circle and oval to a dumbbell-shape contour.

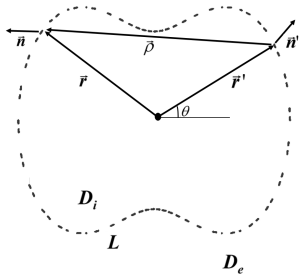

Figure 1. Problem geometry and the parametrization of the contour.

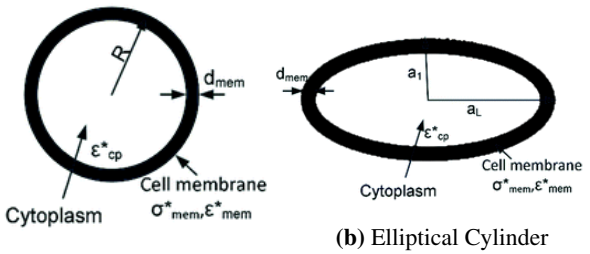

(a) Circular Cylinder **(b)** Elliptical Cylinder

Figure 2. Single shell models for different-shaped biological cells in a homogeneous suspending medium.

The Muller-type boundary integral equations [3] for unknown equivalent currents at the boundary of 2-D scatterer are formulated as follows:

$$U(\vec{r}) + \int_L K_{11}(\vec{r},\vec{r'})U(\vec{r'})ds' - \int_L K_{12}(\vec{r},\vec{r'})V(\vec{r'})ds' = U^i(\vec{r}), \quad (3)$$

$$\frac{1+p}{2}V(\vec{r}) + \int_L K_{21}(\vec{r},\vec{r'})U(\vec{r'})ds' - \int_L K_{22}(\vec{r},\vec{r'})V(\vec{r'})ds' = V^i(\vec{r}), \quad \vec{r} \in L, \quad (4)$$

where $\vec{r} = (x,y)$ and $\vec{r'} = (x',y')$ are the integration and observation points, respectively. U corresponds to the field components E_z or H_z depending on polarization, in the domain D_i (Figure 1). Furthermore, $V(\vec{r'})$ is the limit value of the normal derivative of the total field on the closed contour L of the scatterer from the inner side of it, the normal unit vector $\vec{n}$ is directed to the outer domain D_e, ds' is the elementary arc length, and the constants are $p_{i,e} = \frac{1}{\mu_{i,e}}$ in the E-polarization case and $p_{i,e} = \frac{1}{\varepsilon_{i,e}}$ in the H-polarization case. The primary field and its normal derivative are U^i and V^i, respectively.

The kernels of the MBIE have the following form:

$$K_{11} = \frac{\partial G_i}{\partial n'} - \frac{\partial G_e}{\partial n'}, \; K_{12} = G_i - \frac{p_i}{p_e}G_e, \quad (5)$$

$$K_{21} = \frac{\partial^2 G_i}{\partial n \partial n'} - \frac{\partial^2 G_e}{\partial n \partial n'}, \; K_{22} = \frac{\partial G_i}{\partial n} - \frac{p_i}{p_e}\frac{\partial G_e}{\partial n}, \quad (6)$$

where $G_{(i,e)} = G_{(i,e)}(\vec{r},\vec{r'}) = (i/4)H_0^{(1)}(k_{(i,e)}\rho)$ are the Green functions of the corresponding homogeneous media, $k_i = k_e\sqrt{\varepsilon_i\mu_i}$, and $\rho = |\vec{r} - \vec{r'}|$.

For the case of piece-smooth contour [7], [8], we approximated unknown equivalent currents in (5), (6) with a step-constant function. In our case, when the boundary is smooth and has a regular 2π-periodic parametrization, the Nystrom-type descretization [4], [9] using trigonometric approximation of integrand functions is more convenient, as it leads to exponential convergence of numerical solution.

For the near-field computation, we use (3), which is valid both in D_i and D_e. The far-field pattern can be obtained using the asymptotic expansion of the Hankel function for large arguments [10]:

$$U^{far}(\theta) = \int_L e^{-ik_e(x\cos\theta + y\sin\theta)}\left\{ik_e(\vec{n}\cdot\vec{r})U(\vec{r}) + p\frac{\partial U(\vec{r})}{\partial n}\right\}ds. \quad (7)$$

Bi-static RCS is $\sigma(\theta) = |U^{far}|^2/(4k_e)$.

3 Numerical Results

We consider a single RBC in three different major phases of cell division as depicted in Figure 3. The cell radius is R = 5 μm and the cell membrane thickness is d = 10 nm. The permittivity of the extracellular fluid (outer space) is $\varepsilon_e = 1.77\varepsilon_0$. The permittivities of the cell membrane and cytoplasm are $\varepsilon_{mem} = 1.85\varepsilon_0$, $\varepsilon_{cp} = 1.96\varepsilon_0$, respectively [11]. Numerical simulations are performed at 30 THz, corresponding to the output frequency of a typical CO_2 laser.

In Figure 4, we present the near-field patterns of a single RBC in three diffferent major phases of mitosis under the E-wave excitation at the incidence angle of 72^o with respect to O_x axis. The plots in Figure 5 show the bistatic RCS values of a single RBC at all incidence angles, and it can be seen that the cell shape and orientations have a large influence on the scattering properties of RBCs.

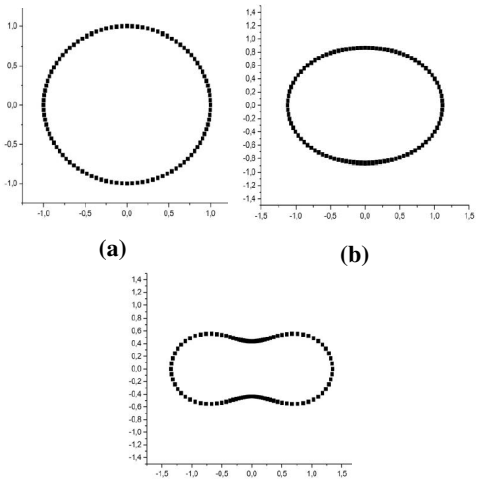

Figure 3. Particle shapes defined by (2) for different values of the parameters, for the symmetric case: a) a = 1, b = 0 (Metaphase); b) a = 1, b = 0.5 (Anaphase); c) a = 1, b = 0.9 (Telophase).

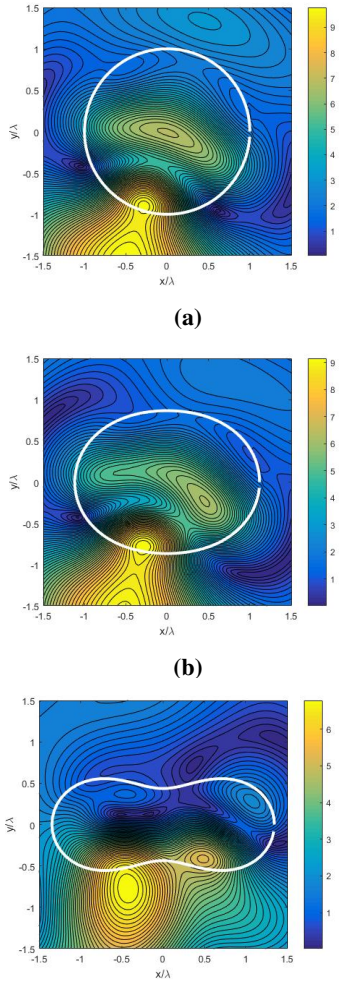

Figure 4. Near-field values of a single RBC; k_0a = 3.14, E-wave excitation: a) a = 1, b = 0; b) a = 1, b = 0.5; c) a = 1, b = 0.9.

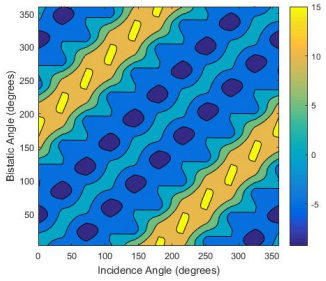

(a)

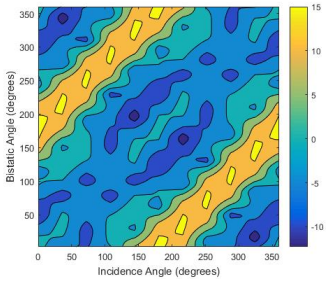

(b)

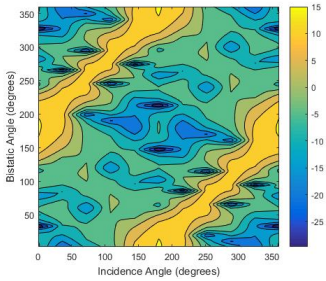

(c)

Figure 5. Bistatic RCS values of a single RBC; E-wave excitation at all incidence angles: a) a = 1, b = 0; b) a = 1, b = 0.5; c) a = 1, b = 0.9.

As depicted in Figure 6, the maximum difference of bistatic patterns between circular and elliptical-shaped red blood cell models is observed at the incidence angles of 117^o and 297^o with respect to O_x axis due to the structure of the ellipse. From Figure 6, it can be seen that the scattering properties of the dumbbell-shaped cell is quite different from the values of the circular cell as compared with the elliptical cell. In other words, total scattering cross section of a dumbbell-shaped cell deviated much more from the circular cell. The amount deviation can be used to detect the different phases of mitosis.

4 Conclusions

In this paper, electromagnetic scattering properties of healthy red blood cells (RBCs) are examined by using Muller boundary integral equation (MBIE) method. Scattering problems involving different RBCs with different orientations are solved accurately and efficiently. By comparing scattering cross section values obtained for different RBCs with different orientations, it may be possible to distinguish different major phases of mitosis of the cell.

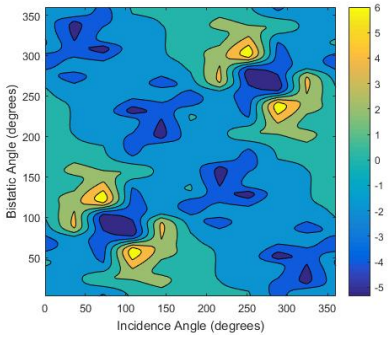

(a)

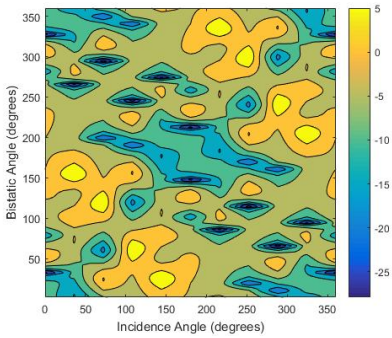

(b)

Figure 6. The difference plots of bistatic patterns for circular and a) elliptical, b) dumbbell-shaped red blood cell models.

5 Acknowledgements

The second author is supported by the Alexander von Humboldt Foundation Fellowship.

References

[1] C. F. Bohren and D. R. Huffman, *Absorption and scattering of light by small particles*, Wiley, New York, 1983.

[2] P. A. Tarasov, M. A. Yurkin, P. A. Avrorov, K. A. Semyanov, A. G. Hoekstra, and V. P. Maltsev, "Optics of erythrocytes," in Optics of Biological Particles, pp. 243-259, Springer, 2007.

[3] C. Muller, *Foundations of the mathematical theory of electromagnetic waves*, Berlin-Heidelberg: Springer-Verlag, 1969.

[4] E. I. Smotrova, V. Tsvirkun, I. Gozhyk, C. Lafargue, C. Ulysse, M. Lebental, and A. I. Nosich, "Spectra, thresholds, and modal fields of a kite-shaped microcavity laser," *J. Opt. Soc. Am. B*, **40**, 6, 2003, pp. 1732-174, doi: 10.1364/JOSAB.30.001732.

[5] T. Sun and H. Morgan, "Single-cell microfluidic impedance cytometry: a review," *Microfluid and Nanofluid.*, **8**, 4, 2010, pp. 423–443, doi: 10.1007/s10404-010-0580-9.

[6] V. I. Smirnov, *A course of higher mathematics, vol. 1*, International Series in Mathematics, Pergamon Press, pp. 200-201, 1964.

[7] I. O. Sukharevsky, A. I. Nosich, and A. Altintas, "Manipulation of backscattering from a dielectric cylinder of triangular cross-section using the interplay of GO-like ray effects and resonances," *IEEE Trans. on Antennas and Propagation*, **63**, 5, 2015, pp. 2162-2169, doi: 10.1109/TAP.2015.2404338.

[8] I. O. Sukharevsky, O. V. Shapoval, A. I. Nosich, and A. Altintas, "Validity and limitations of the median-line integral equation technique in the scattering by material strips of sub-wavelength thickness," *IEEE Trans. on Antennas and Propagation*, **62**, 7, 2014, pp. 3623-3631, doi: 10.1109/TAP.2014.2316295.

[9] D. Colton and R. Kress, *Inverse Acoustic and Electromagnetic Scattering Theory*, Springer, 1998.

[10] G. N. Watson, *A Treatise on the Theory of Bessel functions*, 2d ed., Cambridge University Press, 1966.

[11] P. Jiang, Time domain integral equation-based methods for analyzing electromagnetic scattering from objects residing in lossy media, PhD. thesis, University of Illinois at Urbana Champaign (2007).